Full title: Large-scale exploration of whole-brain structural connectivity in anorexia nervosa: alterations in the connectivity of frontal and subcortical networks

Short title: Whole-brain structural connectivity in anorexia nervosa

Authors: E. Caitlin Lloyd, PhD[1,2,a]; Karin E. Foerde, PhD[1,2]; Alexandra F. Muratore, PhD[1,2]; Natalie Aw, MS[1,2]; David Semanek, BA[1,2]; Joanna E. Steinglass, MD[1,2,b]; Jonathan Posner, MD[3,b]

[a] denotes corresponding author, [b] denotes shared last author

Affiliations:

[1]Department of Psychiatry, Columbia University Irving Medical Center, New York, NY, USA

[2]New York State Psychiatric Institute, New York, New York, NY, USA

[3]Department of Psychiatry, Duke University, Durham, NC, USA

Corresponding author: Dr Caitlin Lloyd

Address: Department of Psychiatry, Columbia University Irving Medical Center, New York, NY, USA.

Phone: 646-774-8201

Email: caitlin.lloyd@nyspi.columbia.edu

Running article title: The structural connectome of anorexia nervosa

Keywords: anorexia nervosa, connectomics, diffusion magnetic resonance imaging, graph theory, structural connectivity, tractography

Abstract:

Background: Anorexia nervosa (AN) is characterized by disturbances in cognition and behavior surrounding eating and weight. The severity of AN combined with the absence of localized brain abnormalities suggests distributed, systemic underpinnings that may be identified by using diffusion-weighted MRI (dMRI) and tractography to reconstruct white matter pathways.

Methods: dMRI data acquired from female patients with AN (n = 148) and female healthy controls (HC; n = 119), aged 12-40 years, were combined across five studies. Probabilistic tractography was completed, and full cortex connectomes describing streamline counts between 84 brain regions generated and harmonized. Graph theory methods were used to describe alterations in network organization in AN. The network-based statistic tested between-group differences in brain subnetwork connectivity. The metrics strength and efficiency indexed the connectivity of brain regions (network nodes), and were compared between groups using multiple linear regression.

Results: Individuals with AN, relative to HC, had reduced connectivity in a network comprising subcortical regions and greater connectivity between frontal cortical regions ($p < 0.05$, FWE corrected). Node-based analyses indicated reduced connectivity of subcortical regions in patients relative to HC ($p < 0.05$, permutation corrected). Severity of illness, assessed by BMI, was associated with subcortical connectivity ($p < 0.05$, uncorrected).

Conclusions: Structural connectivity analyses identified reduced connectivity of subcortical networks and regions, and stronger cortical network connectivity, amongst individuals with AN relative to HC. These findings are consistent with alterations in feeding and executive control circuits in AN, and may direct hypothesis-driven research into mechanisms of persistent restrictive eating behavior.

Introduction

Anorexia nervosa (AN) is a serious illness characterized by extreme food restriction and disturbances in cognition surrounding eating and weight (1). The illness is associated with high rates of mortality (2), medical and psychiatric morbidity (3, 4), and severe decrements in quality of life (5). Treatment for AN is challenging, with disappointing remission rates and high rates of relapse (6). The severity of the psychiatric symptoms in AN makes it somewhat puzzling that mechanisms of illness have not been more easily localized, despite increasing research into the underlying neural pathology (7). The inconclusive findings from hypothesis-driven studies, to-date, leads to the data-driven approach in this study. In this study we aim to examine brain-wide structural connectivity by leveraging advances in network-based models of the brain, and a state-of-the-art probabilistic approach to diffusion-weighted MRI (dMRI) tractography.

White matter connects spatially distinct brain regions, creating the structural connections that support coordinated neural activation. Thus, white matter connections are the structural architecture underlying neural networks (8, 9), and disturbances in this architecture, or connectivity, may in turn reflect abnormal functioning of neural networks. White matter tracts of the brain can be delineated in vivo using dMRI (10), and as such, dMRI may offer a useful tool for advancing circuit-based inquiry into disease mechanisms in AN.

To date, several dMRI studies of AN have been conducted and have generated interesting findings (for review, see (11)). Despite the promise of this work, dMRI studies in AN have been limited in several ways. First, most dMRI studies of AN have focused on regional white matter microstructure. Microstructural measurements provide information about the integrity of white

matter within a given brain region, but do not assess region-to-region connectivity. Conversely, diffusion tractography is a dMRI approach that captures connectivity by reconstructing white matter pathways throughout the brain. Several diffusion tractography studies of AN have been reported, but here too, there have been important limitations. Most notably, tractography studies of AN have been constrained by small sample sizes, and consistent findings across studies have not emerged (11-13). The single tractography study that had a relatively large sample (n= 96 AN and 96 HC (14)) used deterministic tractography, an approach that assumes that all white matter fibers within a voxel are oriented in the same direction. This assumption does not comport with histological tracings that indicate that white matter often contains complex fiber architectures such as bending or crossing fibers (15, 16). Therefore newer approaches to tractography use probabilistic algorithms to model multiple fiber orientations per voxel, to provide more biologically accurate representations of white matter pathways (17). In sum, while dMRI offers a promising tool for studying brain architecture, prior dMRI studies of AN have been limited by methodological approaches.

The current study addresses the aforementioned limitations, and differs from the majority of prior dMRI research by adopting a data driven, or hypothesis-generating, approach. Discovery-based, or data driven, approaches are particularly useful when prior knowledge, upon which hypotheses are formulated, is limited—as is the case with the knowledge of white matter architecture in AN. Whilst testing directed hypotheses can be well suited for identifying disease mechanisms, the narrow lens inherent to hypothesis testing can miss unanticipated but meaningful differences in brain architecture. Data-driven approaches, on the other hand, can

direct the development of questions concerning the possible underpinnings of disease, which in subsequent studies can be subjected to hypothesis testing.

Leveraging a large sample size and techniques to handle multiple comparisons, the current study obviates a central concern of data-driven approaches—generating false-positive results when sample sizes are small. In particular, a graph theory approach is used to explore structural connectivity in AN. The application of mathematical graph theory in neuroscience has led to a network model of the brain: the structural connectome, which comprises a set of "nodes" (brain regions) and "edges" (pairwise structural connections between all regions of the brain (18)). Coupled with tractography, graph theory provides an analytic framework for describing structure within the brain, and even the organization of the whole brain. The approach lends itself to studying the neural architecture that arises across multiple connections, rather than the strength of a discrete pairwise connection. Graph theory analytics can thus provide information about network-level abnormalities in brain organization that may underlie psychopathology.

Methods

Analysis of dMRI data collected from 267 participants via five cross-sectional studies (12, 19-22) was undertaken. Data from a subsample of participants from one study (n= 22 AN and 18 HC) were included in a prior publication comparing specific frontostriatal tracts between individuals with AN and HC (12).

Participants

Participants were 148 females who met DSM-5 criteria for AN, and 119 age-matched female HC. Participants were between the ages of 12 and 40 years. Exclusion criteria were the same across studies: current substance use disorder, lifetime psychotic disorder, history of a neurological disorder/injury, estimated IQ less than 80, and contraindications to MRI. Additional exclusion criteria for HC included any current/past major psychiatric illness, serious or unstable medical condition, and body mass index (BMI) outside of the normal range (18.5-25 kg/m^2). Among AN, participants were free from psychotropic medication use at the time of MRI scanning, except for 11 patients taking antidepressant medication. Eating disorder diagnoses were made by the Eating Disorder Examination (23) or Eating Disorder Diagnostic Assessment for DSM-5 (24). Co-occurring diagnoses were assessed by Structured Clinical Interview for DSM-IV or DSM-5 for adults (25, 26), and by the Schedule for Affective Disorders and Schizophrenia for School-Aged Children for adolescents (27). Height and weight were measured on the day of the MRI scan (for calculation of BMI), by stadiometer and balance beam scale respectively. Each study was approved by the New York State Psychiatric Institute (NYSPI) Institutional Review Board. Researchers provided a complete description of the study to participants. Adult participants provided written informed consent, and adolescents provided written assent with parental consent.

Amongst patients with AN, 85 (57.4%) were diagnosed with the restricting subtype. Adults with AN were receiving specialized inpatient eating disorder treatment at NYSPI. Adolescents were receiving inpatient or outpatient treatment. HC were recruited from the community.

MRI procedures

Scanning parameters

The MRI scanner and DWI scanning parameters are described in the Supplement (**Table S1**) for each of the five studies. All DWI acquisitions were single shell.

MRI Image processing

Anatomical images

Structural images were processed using the automated Freesurfer pipeline (28, 29), which includes motion correction, brain extraction, Talairach transformation and intensity normalization. Grey matter regions were parsed into 84 distinct regions based on the Desikan-Killany atlas (30).

The parcellated image was used to generate a five-tissue type image, in which white matter, cortical and subcortical grey matter, cerebral spinal fluid (CSF), and pathological tissue are distinguished. Anatomical images were warped into diffusion space using a rigid body transformation performed with FSL's flirt method (31, 32), followed by a non-linear normalization using ANTS (33, 34), and resampled such that the voxel size was 1.25 mm^3.

Diffusion images

Each scan was visually checked for artifacts prior to image pre-processing, and volumes containing artifacts were removed. Participants' data were excluded if more than 25% of the total volumes were removed (n = 3 AN and 0 HC). A fully automated image pre-processing pipeline implemented in MRtrix3 (35) was applied to the data, including: denoising, gibbs-artifact removal, B0 susceptibility-induced distortion correction, eddy current and motion correction (using the FSL eddy tool; (36)), and B1 field inhomogeneity correction (using the ANTS N4

algorithm; (37)). Preprocessed dMRI data were resampled to an isotropic voxel size of 1.25 mm^3. Motion was quantified with average framewise displacement across the dMRI scan and did not differ between AN and HC groups: HC=0.16 (SD=0.1), AN = 0.18 (SD=0.15); t(265) = 1.09, p = 0.276. Details of average framewise displacement by diagnostic group and study are available in the Supplement (**Table S2**).

Reconstruction of White Matter - Probabilistic Tractography

To delineate the white matter pathways of the brain, anatomically-constrained probabilistic tractography was completed using a standard MRtrix3 pipeline (35). Under this approach (described fully in the Supplemental material) plausible white matter pathways are reconstructed by propagating along estimates of voxel fiber orientation distributions (using the iFOD2 tracking algorithm (38)). Fiber distributions in each voxel were recovered using multi-shell multi-tissue constrained spherical deconvolution (39). 20,000,000 streamlines between 10 and 250 mm were generated, and filtered to 5,000,000 using the SIFT algorithm, which maximizes the fit between the reconstructed streamlines and dMRI data.

Constructing structural connectomes

To create brain networks (i.e., structural connectomes), a node was assigned to each of the 84 regions from the anatomical parcellation. For each participant, the number of streamlines between all possible pairs of regions, or nodes (Ni, Nj), was counted, with streamline endpoints mapped to nodes within a 4mm radius of the endpoint. Streamline counts quantify connectivity strength and provided edge values for individual participant networks that describe whole-brain connectivity. When no streamlines connected a pair or regions, the edge value was set to 0.

To remove effects of differences in scanner/scan parameters across and within studies, individual brain networks (or structural connectomes) were harmonized using the R implementation of neuroCombat (40, 41). To retain effects of diagnosis, age and BMI on the brain networks, the variables were specified as covariates in the harmonization model. In exploratory analyses probing subtype differences in structural connectivity, the harmonization model was applied to data from AN patients only, and included subtype as an additional covariate.

Following recent recommendations, brain networks were not thresholded prior to completing analyses (42).

Data analysis

Streamline counts between brain regions constituted the measure of connectivity in all network-based and node-based analyses.

Network-based statistic (43)

Subnetwork connectivity within the structural connectome was compared between AN and HC groups using the network-based statistic method implemented in Matlab (https://sites.google.com/site/bctnet/comparison/nbs; (44)). This method assesses whether groups show greater or reduced streamline counts in constellations of connected tracts, or subnetworks. First tracts differing in streamline count between groups at a t-score threshold of greater than 3.1 (corresponding to a p-value of 0.001) are identified. Next, components, or sets of connected tracts meeting the t-score criteria, are identified. The null distribution of the maximum component size is empirically estimated using a permutation approach. P-values for the hypothesis that observed components (i.e., those identified in the unpermuted data) are larger

than expected should there be no between-group difference in subnetwork connectivity can then be derived. 10,000 permutations were specified, and identified components were significant at a family-wise error corrected rate of $p < 0.05$. The network-based statistical analysis was completed for the contrasts HC > AN, and AN > HC; p-values were Bonferroni-corrected for two tests. Models were adjusted for age, motion and study. Study was included as a covariate given the potential for residual batch effects to remain following harmonization.

Node-based analyses

Strength and *efficiency*, which describe the connectivity properties of brain regions (nodes), were computed for each network node, using the BCT toolbox (https://sites.google.com/site/bctnet/) in Matlab (44, 45). Strength is calculated as the total number of connections (streamlines) of each node. Efficiency describes the ease at which information can move from one region to another within a network of the node's neighbours; "ease" referring to fewer intermediary nodes (46). To calculate efficiency, the inverse of the shortest path length between all nodes directly connected to the node in question was determined and averaged. Path length was defined as the inverse of streamline count. The contribution of a given path to the efficiency calculations was proportionate to the streamline count between the path nodes and the node for which efficiency was calculated (i.e., the average was weighted) (47). *Global efficiency*, the ease at which information can move from one region to any other region on average across the whole brain, was also calculated (46).

Node characteristics were compared between AN and HC in linear regression models adjusted for age, motion and study. Permutation tests established statistical significance and corrected for

multiple comparisons across the 84 nodes (applying the minP method), using the R package Permuco (48). 10,000 permutations for each test were specified; the Freedman-Lane procedure managed effects of nuisance variables (age, motion and study). A linear regression model adjusted for age, motion and study compared AN and HC groups on the global efficiency metric.

The tractography, connectome generation, node metric calculation and analysis procedures are detailed in **Figure 1**.

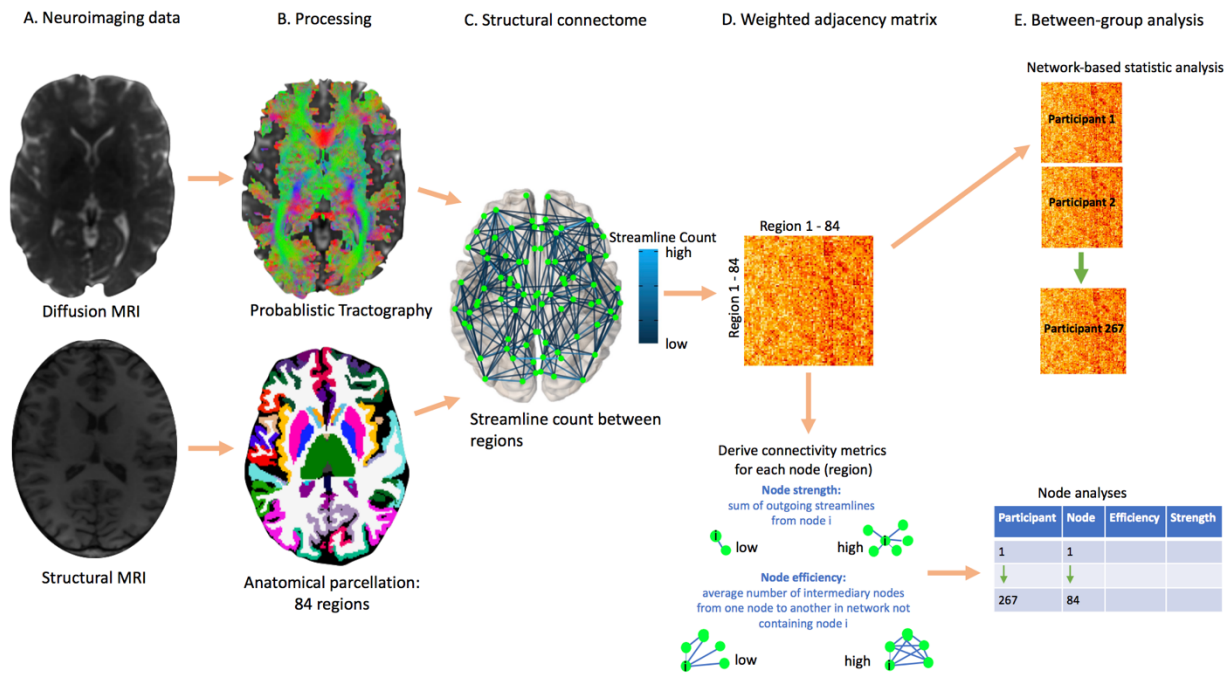

Figure 1: Neuroimaging and analysis methods
For each participant, a diffusion MRI and structural MRI scan were acquired (panel A). White matter tracts in the brain were reconstructed using a probabilistic tracking algorithm applied to diffusion MRI data, and the structural brain image was parcellated into 84 regions (panel B). Combining the tractography output with the brain parcellation allowed the creation of a structural connectome for each participant, which described the number of streamlines between each pair of regions (panel C). This information was represented in a weighted adjacency matrix, which was used to calculate node metrics (panel D). Anorexia nervosa and healthy control groups were compared on the strength of structural connections and node metrics, across the whole brain (panel E).

The main analyses probing group differences in brain network attributes were repeated using unharmonized data, to verify whether findings were consistent across different methods for combining data from the five studies.

Exploratory analyses

Subnetwork components that significantly differed between groups ($p < 0.05$, corrected) were tested for their association with illness severity, indexed by BMI and illness duration, within the AN group. For each component reaching statistical significance, the mean number of streamlines across edges of these components was calculated. BMI percentile, which indexes how an individual's BMI compares to that of others of the same age and sex, is a more appropriate marker for weight status in childhood and adolescence. Thus, BMI percentile was calculated for participants aged up to 19 years. To combine BMI measurements across adults (aged over 19 years) and adolescents (aged 19 years and below) of the study, standardized scores (mean centred and scaled by the standard deviation) were calculated in the two groups, using BMI for adults, and BMI percentile for adolescents. These standardized scores were then combined to create the standardized BMI variable. Network component connectivity metrics were regressed onto standardized BMI and illness duration, in separate models. Using the same method, node metrics that differed between groups were tested for their association with clinical variables amongst individuals with AN. All statistical models were adjusted for motion, age and study. Models involving the regression of illness duration were additionally adjusted for standardized BMI. Model predictors and outcomes (aside from the already standardized BMI variable) were mean centred and scaled, for comparison of effect estimates across exploratory analyses.

Component connectivity and node metrics that differed between AN and HC groups were compared between AN subtypes, in linear regression models adjusted for motion, age, study, and standardized BMI.

We did not account for multiple comparisons in exploratory analyses.

Code and data availability

The code for dMRI data preprocessing, tractography, and analysis steps is available on github: https://github.com/CaitlinLloyd/Anorexia.Nervosa_Tractography. Data for between group differences in streamline counts between all pairs of regions are available as Supplementary material (see Supplementary Tables file).

Results

Participant characteristics

Participant characteristics are displayed in **Table 1**. For a summary of results by study and diagnosis, see the Supplement (**Table S2**). Groups were well-matched in age, and differed as expected in BMI and all clinical variables.

Table 1: Demographic and clinical characteristics

Variable	**HC (n = 119)**	**AN (n = 148)**
	Mean ± SD	Mean ± SD
Age (years)	21.03 ± 5.11	20.34 ± 6.21
BMI (kg/m^2)[a*]	21.49 ± 1.69 (n = 77)	16.08 ± 1.97 (n = 70)
BMI percentile (%)[b*]	47.74 ± 23.38	9.6 ± 10.5

	(n = 42)	(n = 78)
EDEQ Global score*	0.27 ± 0.39	3.9 ± 1.54
Illness Duration (months)	NA	58.15 ± 69.61

[a] BMI information presented for participants **over 19**
[b] BMI percentile information presented for participants **19 and under**
* p-value for between group difference < 0.001
BMI: Body mass index; EDEQ: Eating disorder examination questionnaire

Network-based statistic

The network-based statistic indicated one component with stronger connectivity amongst HC compared to AN (**Figure 2, Panel A**). This component included 11 connections between subcortical regions (p = 0.026). Conversely, the network-based statistic indicated one component that was stronger amongst individuals with AN relative to HC (**Figure 2, Panel B**). This component included 8 connections between regions generally located in the frontal cortex (p = 0.042). Details of average connectivity within the subcortical and cortical components, by study and diagnosis, are presented in the Supplement (**Table S3, Figures S1 and S2**).

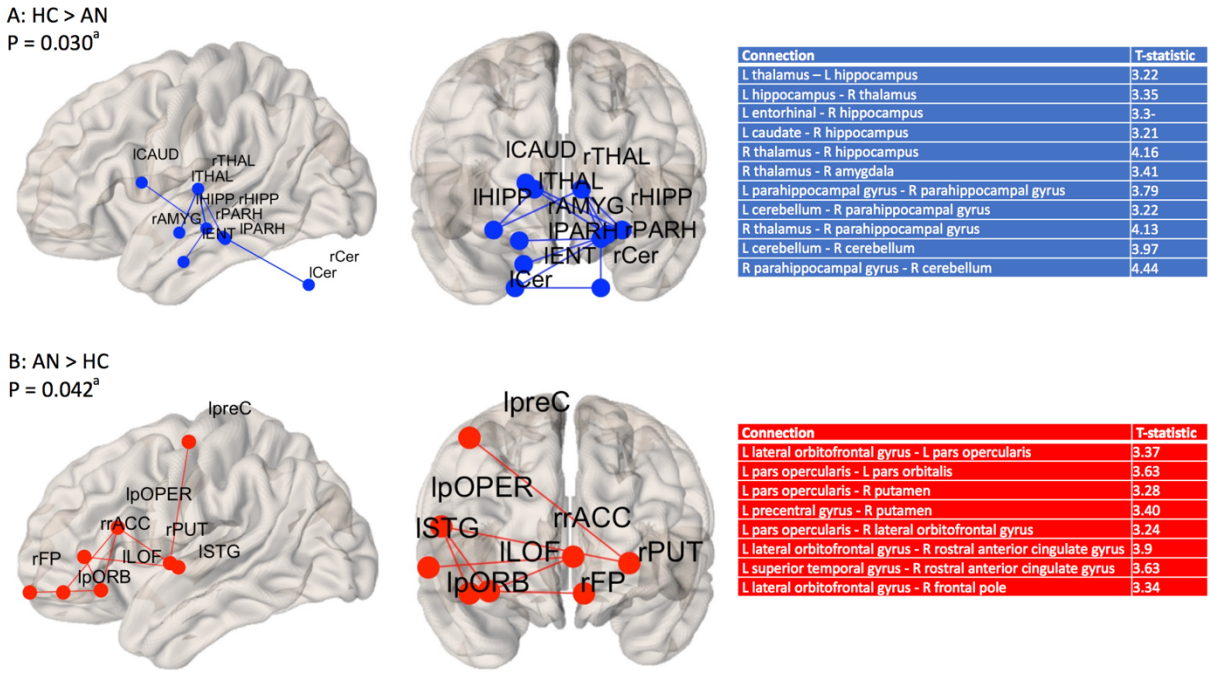

Connection	T-statistic
L thalamus – L hippocampus	3.22
L hippocampus - R thalamus	3.35
L entorhinal - R hippocampus	3.3-
L caudate - R hippocampus	3.21
R thalamus - R hippocampus	4.16
R thalamus - R amygdala	3.41
L parahippocampal gyrus - R parahippocampal gyrus	3.79
L cerebellum - R parahippocampal gyrus	3.22
R thalamus - R parahippocampal gyrus	4.13
L cerebellum - R cerebellum	3.97
R parahippocampal gyrus - R cerebellum	4.44

Connection	T-statistic
L lateral orbitofrontal gyrus - L pars opercularis	3.37
L pars opercularis - L pars orbitalis	3.63
L pars opercularis - R putamen	3.28
L precentral gyrus - R putamen	3.40
L pars opercularis - R lateral orbitofrontal gyrus	3.24
L lateral orbitofrontal gyrus - R rostral anterior cingulate gyrus	3.9
L superior temporal gyrus - R rostral anterior cingulate gyrus	3.63
L lateral orbitofrontal gyrus - R frontal pole	3.34

Figure 2: Weaker subcortical connectivity and stronger cortical connectivity among individuals with AN
Panel A) Component comprising tracts with higher streamline counts in HC compared to patients with AN. Panel B) Component comprising tracts with higher streamline counts in patients with AN compared to HC. AN: anorexia nervosa, HC: healthy controls, lLOF: left lateral orbitofrontal gyrus, lpOPER: left pars opercularis, lpORB: left pars orbitalis, lpreC: left precentral gyrus, lSTG: left superior temporal gyrus' rFP: right frontal pole, rPUT: right putamen, rrACC: right rostral anterior cingulate gyrus, lCer: left Cerebellum, lFP: left frontal pole, lLOF: left lateral orbitofrontal, lPARH: left parahippocampal gyrus, lTHAL: left thalamus, rHIPP: right hippocampus, rPARH: right parahippocampal gyrus, rTHAL: right thalamus.
[a] P-values are Bonferonni-corrected for multiple comparisons.

Node-based analyses

Node-based analyses indicated that individuals with AN, relative to HC, had reduced strength of the left hippocampus (B = -2367.69, [95% CI: -3549.32, -1186.06], p = 0.008), left cerebellum (B = -2420.77, 95% CI: [-3646.02, -1195.52], p = 0.024), left parahippocampal gyrus (B = -1284.7, 95% CI: [-1992.31, -577.08], p = 0.024), right cerebellum (B = -2361.14, 95% CI: [-3618.19,-1104.09], p = 0.024), and greater strength of the left lateral occipital gyrus (B = 2186.39, 95% CI: [901.84, 3470.95], p = 0.024). There were no significant differences in local efficiency between groups, and global efficiency also did not differ between groups (B = 3.31, 95% CI: [-10.78, 17.40], p = 0.64). Results of all node-based analyses are reported in the Supplement (**Tables S4 and S5**).

Unharmonized data analyses

Analyses with unharmonized data yielded outcomes that were consistent (in direction, size and significance) with outcomes of harmonized data analyses. Full results are reported in the Supplement (**Tables S7-S9**).

Association between structural connectome metrics and severity of illness

Results of exploratory analyses are presented in **Table 2**. Amongst individuals with AN, the standardized BMI variable was positively associated with connectivity within the subcortical component (B = 0.20, 95% CI: [0.04, 0.36], p = 0.016; **Figure 3**). Illness duration was not significantly associated with any of the structural connectivity measures.

Table 2: Outcomes of linear regression analyses exploring associations of illness severity markers with identified structural connectome differences amongst individuals with AN

Predictor variable[a]	**Association with BMI(kg/m^2)**[bd]		**Association with Illness Duration**[c]	
Structural connectivity metric	B [95% CI]	P-value	B [95% CI]	P-value
Subcortical component connectivity	0.2 [0.04,0.36]	0.02	-0.02 [-0.14,0.1]	0.78
Cortical component connectivity	-0.14 [-0.3,0.02]	0.10	0.01 [-0.11,0.13]	0.88
Strength of left parahippocampal gyrus	0.1 [-0.07,0.26]	0.25	-0.02 [-0.13,0.1]	0.77
Strength of left cerebellem	0.04 [-0.13,0.2]	0.67	0 [-0.11,0.12]	0.98
Strength of left hippocampus	0.1 [-0.06,0.26]	0.23	-0.05 [-0.17,0.07]	0.40
Strength of right lateral occipital gyrus	0.03 [-0.14,0.2]	0.76	0.08 [-0.04,0.2]	0.21
Strength of right cerebellem	0.06 [-0.11,0.22]	0.50	-0.01 [-0.13,0.11]	0.83

BMI: body mass index.
[a]Predictors and outcome variables were mean centered and scaled.
[b]Models adjusted for age, motion and study.
[c]Models adjusted for age, motion, study, and the scaled BMI variable.
[d]The BMI variable combined scaled BMI scores calculated in adults of the sample (aged over 19 years) with scaled BMI percentile scores calculated in adolescents (aged 19 years and below).

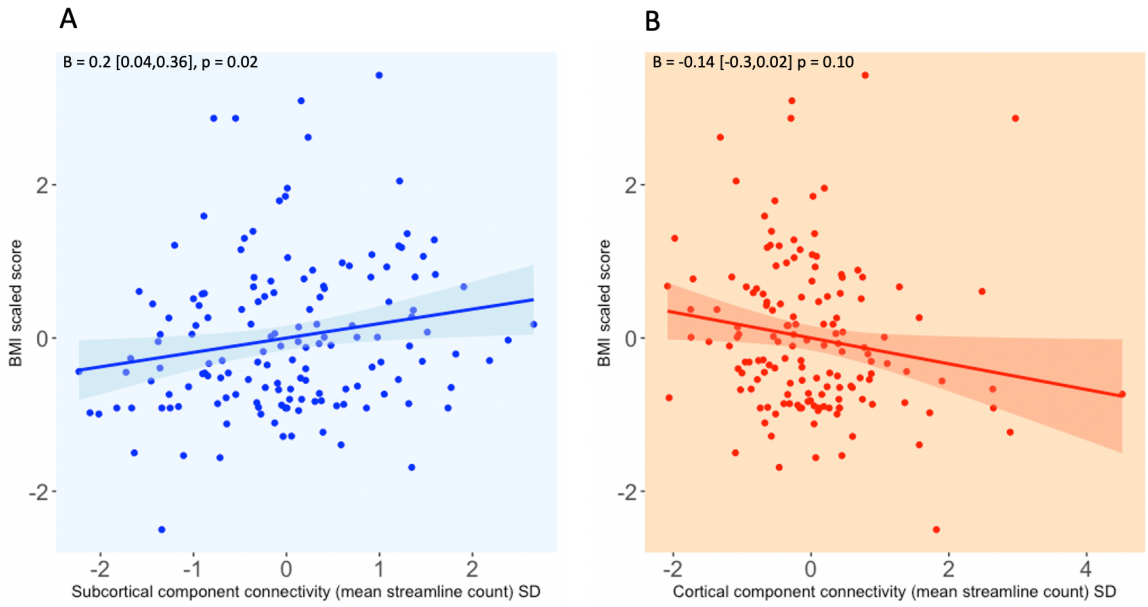

Figure 3: Associations between subnetwork connectivity and BMI amongst individuals with AN Panel A) Average streamline count in the subcortical network plotted against scaled BMI score in the AN sample. Panel B) Average streamline count in the cortical network plotted against scaled BMI score in the AN sample. The beta value indexes the strength of association between subnetwork connectivity and scaled BMI score, and was calculated by regressing the BMI variable onto the average streamline count within each subnetwork in a model adjusted for age, motion and study. Average streamline counts for each subnetwork were standardized (demeaned and scaled) within the AN group.

Subtype differences

Individuals with AN binge-eating-purging subtype had greater strength, or connectivity, of the right cerebellum relative to individuals with AN restricting subtype. There were no other significant structural connectivity differences between subtypes (Supplementary material, **Table S10**).

Discussion

The current study describes white matter connectivity of the brain in a large group of individuals with AN, as compared with HC, using state-of-the-art data processing and analytical methods. To obtain a more biologically plausible representation of complex white matter fiber architecture, anatomical connections of the brain were reconstructed using probabilistic

tractography. To minimize bias arising from differences in MRI scanners across studies, data were harmonized using well-validated methods. Graph theory analyses using network-based and node-based approaches produced convergent findings that suggest increased cortical connectivity and decreased subcortical connectivity among individuals with AN as compared with HC.

A network-based statistic analysis indicated that, relative to HC, individuals with AN had enhanced connectivity in a cluster of tracts connecting regions of the frontal cortex. In contrast, patients showed reduced connectivity within a network of subcortical brain regions relative to HC, and lower connectivity in this network was associated with lower BMI amongst the AN sample. Node-based analyses identified that a number of the same subcortical regions (hippocampus, parahippocampal gyrus, cerebellum) were less well-connected in general (i.e., showed weaker connectivity with all regions of the brain) amongst individuals with AN relative to HC. These data-driven, whole-brain findings suggest organizational differences in the brain between individuals with AN and HC that could explain core clinical features of the disorder.

The subcortical network that showed alterations in AN overlaps with reward and feeding circuits, and included connections between thalamic, hippocampal, striatal and amygdala regions. Reduced connectivity within this system could conceivably impact the desire to eat, as proposed by “bottom-up” models of illness. The association between subcortical network connectivity and BMI amongst the AN group could reflect this possibility. In contrast, the heightened frontal connectivity observed amongst individuals with AN is consistent with “top-down” models of illness. These models emphasize greater functioning within frontal circuits (49, 50), which is suggested to underlie the high levels of cognitive control and behavioral rigidity observed in

patients (51). One hypothesis generated by the current findings is that persistent dietary restriction in AN stems from brain network alterations via a combination of reduced appetitive motivation and inflexible cognition/behavior surrounding eating. This hypothesis can be tested in future research by examining whether the identified network-level structural changes are related to eating behavior.

Several regions of the subcortical network that showed reduced connectivity amongst individuals with AN (i.e., caudate, thalamus, hippocampus) are considered "hubs", or regions that are typically densely connected. Hubs are particularly well-connected with each other, causing the so-called "rich-club" structure of the brain that ensures a system able to balance segregation and integration for optimal information processing (52). The thalamus and hippocampus also showed reduced whole-brain connectivity in node-based analyses. These results may reflect alterations in more global properties of brain organization that affect cognition and behavior beyond the motivation to eat. This could be explored in future studies able to link indices of diffuse brain organization with assessments of general psychopathology (e.g., anxiety, depression) and cognitive functions such as memory and learning.

Our findings are consistent with prior dMRI studies of white matter architecture in AN. Several studies have reported that individuals with AN, as compared with HC, have greater integrity within frontal portions of the inferior fronto-occipital fasciculus (53, 54), and reduced integrity of white matter in the fornix (11). The inferior fronto-occipital fasciculus traverses the inferior frontal and medial prefrontal regions in which elevated connectivity was seen amongst individuals with AN in the current study. The fornix comprises the major output tract of the

hippocampus, and encapsulates connections of the subcortical component showing reduced connectivity in AN (e.g., tracts between hippocampus, thalamus, parahippocampal cortex and entorhinal cortex). These studies align with the conclusion that there is greater processing within frontal networks, and reduced processing in subcortical networks, in AN.

The current findings differ somewhat from prior investigations of region-to-region white matter connectivity. Two prior studies testing group differences in individual tracts reported stronger connectivity in intra-hemispheric frontostriatal tracts amongst individuals with AN, both between the nucleus accumbens and OFC (12, 55), and between the putamen and motor areas (13). These differences were not found in the current study, which could result from the unit of analysis here being constellations of connected white matter connections rather than individual tracts. The only other large-scale investigation of the structural connectome in AN probed (as we did) differences in constellations of white matter connections (or subnetworks). This earlier study reported no between-group differences in network connectivity based on streamline counts, but did observe greater integrity of white matter in occipital-parietal regions amongst individuals with AN (14). The tract reconstruction method of the prior study assumed the presence of a single fiber direction per voxel, whilst the multi-fiber probabilistic approach implemented herein produces a more biologically accurate reconstruction of white matter pathways (15-17). Regardless, replication of the tract reconstruction and analytical methods of the current study are warranted to confirm the reliability of findings.

This study has multiple strengths. It is the largest diffusion tractography investigation of AN to date, and used current best practices for dMRI data processing and data analysis. Nonetheless,

there are several limitations that should be considered when interpreting results. First, the data are cross-sectional, meaning causes and consequences of starvation cannot be parsed. Longitudinal studies may provide insight into whether the structural connectivity abnormalities associated with AN in this study predict remission versus persistence of illness, and/or whether they normalize when weight is restored to the normal range. This would help with interpreting the correlation between subnetwork connectivity and BMI in the current study. Second, dMRI data were not optimal for constrained spherical deconvolution-based tractography. Ideally, dMRI scans would have been acquired with higher b-values (e.g., 3000), for more precise estimation of fiber orientation distributions within a given voxel. However even at low b-values, constrained spherical deconvolution-based tractography outperforms methods assuming a single-fiber orientation within each voxel, in terms of producing an anatomically accurate reconstruction of white matter pathways(56). Third, data harmonization does not completely remove batch effects, and collecting all dMRI data in one study would have been ideal.

In summary, this large-scale investigation of whole-brain structural connectivity in patients with AN implemented advances in diffusion tractography and graph theory methods to yield information about the neural architecture underlying AN. Individuals with AN had reduced connectivity of and between subcortical regions, and elevated connectivity between frontal regions. The identified connectivity profile hints at weaker processing within networks supporting feeding behavior, and greater processing within networks supporting executive function. This combination may drive restrictive eating behavior, opening new avenues for hypothesis-driven longitudinal research in AN.

Disclosures

Dr. Steinglass reports receiving royalties from UpTo Date. Dr. Posner has received support from Takeda (formerly Shire), Aevi Genomics, and Innovation Sciences. Dr Lloyd, Dr Foerde, Ms Aw, Mr Semanek, and Dr Muratore have no conflicts of interest to report.

The article has been posted on the bioRxiv preprint server.

References

1. American Psychiatric Association. Diagnostic and statistical manual of mental disorders (DSM-5®): American Psychiatric Pub; 2013.
2. Arcelus J, Mitchell AJ, Wales J, Nielsen S. Mortality rates in patients with anorexia nervosa and other eating disorders. A meta-analysis of 36 studies. Arch Gen Psychiatry. 2011;68(7):724-31.
3. Mehler PS, Brown C. Anorexia nervosa - medical complications. J Eat Disord. 2015;3:11.
4. Ulfvebrand S, Birgegård A, Norring C, Högdahl L, von Hausswolff-Juhlin Y. Psychiatric comorbidity in women and men with eating disorders results from a large clinical database. Psychiatry Res. 2015;230(2):294-9.
5. Ágh T, Kovács G, Supina D, Pawaskar M, Herman BK, Vokó Z, et al. A systematic review of the health-related quality of life and economic burdens of anorexia nervosa, bulimia nervosa, and binge eating disorder. Eat Weight Disord. 2016;21(3):353-64.
6. Berends T, Boonstra N, van Elburg A. Relapse in anorexia nervosa: a systematic review and meta-analysis. Current opinion in psychiatry. 2018;31(6):445-55.
7. Glashouwer KA, Brockmeyer T, Cardi V, Jansen A, Murray SB, Blechert J, et al. Time to make a change: A call for more experimental research on key mechanisms in anorexia nervosa. European Eating Disorders Review. 2020;28(4):361-7.
8. Shen K, Hutchison RM, Bezgin G, Everling S, McIntosh AR. Network structure shapes spontaneous functional connectivity dynamics. Journal of Neuroscience. 2015;35(14):5579-88.
9. Horn A, Ostwald D, Reisert M, Blankenburg F. The structural–functional connectome and the default mode network of the human brain. Neuroimage. 2014;102:142-51.
10. Le Bihan D, Breton E, Lallemand D, Grenier P, Cabanis E, Laval-Jeantet M. MR imaging of intravoxel incoherent motions: application to diffusion and perfusion in neurologic disorders. Radiology. 1986;161(2):401-7.
11. Gaudio S, Carducci F, Piervincenzi C, Olivo G, Schiöth HB. Altered thalamo–cortical and occipital–parietal–temporal–frontal white matter connections in patients with anorexia and bulimia nervosa: a systematic review of diffusion tensor imaging studies. Journal of psychiatry & neuroscience: JPN. 2019;44(5):324.
12. Cha J, Ide JS, Bowman FD, Simpson HB, Posner J, Steinglass JE. Abnormal reward circuitry in anorexia nervosa: A longitudinal, multimodal MRI study. Human brain mapping. 2016;37(11):3835-46.
13. Tadayonnejad R, Pizzagalli F, Murray SB, Pauli WM, Conde G, Bari AA, et al. White matter tracts characteristics in habitual decision-making circuit underlie ritual behaviors in anorexia nervosa. Scientific Reports. 2021;11(1):15980.
14. Geisler D, King JA, Bahnsen K, Bernardoni F, Doose A, Müller DK, et al. Altered White Matter Connectivity in Young Acutely Underweight Patients With Anorexia Nervosa. Journal of the American Academy of Child & Adolescent Psychiatry. 2021.
15. Tournier JD, Calamante F, Connelly A. MRtrix: Diffusion tractography in crossing fiber regions. International Journal of Imaging Systems and Technology. 2012;22(1):53-66.
16. Farquharson S, Tournier J-D, Calamante F, Fabinyi G, Schneider-Kolsky M, Jackson GD, et al. White matter fiber tractography: why we need to move beyond DTI. Journal of neurosurgery. 2013;118(6):1367-77.

17. Tournier J-D, Mori S, Leemans A. Diffusion tensor imaging and beyond. Magnetic resonance in medicine. 2011;65(6):1532-56.
18. Sporns O, Tononi G, Kötter R. The human connectome: a structural description of the human brain. PLoS computational biology. 2005;1(4):e42.
19. Foerde K, Steinglass JE, Shohamy D, Walsh BT. Neural mechanisms supporting maladaptive food choices in anorexia nervosa. Nat Neurosci. 2015;18(11):1571-3.
20. Foerde K, Schebendach JE, Davis L, Daw N, Walsh BT, Shohamy D, et al. Restrictive eating across a spectrum from healthy to unhealthy: behavioral and neural mechanisms. Psychological Medicine. 2020:1-10.
21. Uniacke B, Wang Y, Biezonski D, Sussman T, Lee S, Posner J, et al. Resting-state connectivity within and across neural circuits in anorexia nervosa. Brain and behavior. 2019;9(1):e01205.
22. Lloyd EC, Foerde, K., Posner, J.P., & Steinglass, J., editor Longitudinal assessment of neural circuits in adolescents with anorexia nervosa: preliminary behavioral findings. Eating Disorders Research Society annual meeting; 2020.
23. Fairburn CG, Wilson GT, Schleimer K. Binge eating: Nature, assessment, and treatment: Guilford Press New York; 1993.
24. Sysko R, Glasofer DR, Hildebrandt T, Klimek P, Mitchell JE, Berg KC, et al. The eating disorder assessment for DSM-5 (EDA-5): Development and validation of a structured interview for feeding and eating disorders. The International journal of eating disorders. 2015;48(5):452-63.
25. Team RC. R: A Language and Environment for Statistical Computing. R Foundation for Statistical Computing; 2017.
26. First MB. Structured clinical interview for the DSM (SCID). The encyclopedia of clinical psychology. 2014:1-6.
27. Kaufman J, Birmaher B, Brent D, Rao U, Flynn C, Moreci P, et al. Schedule for affective disorders and schizophrenia for school-age children-present and lifetime version (K-SADS-PL): initial reliability and validity data. Journal of the American Academy of Child & Adolescent Psychiatry. 1997;36(7):980-8.
28. Fischl B. FreeSurfer. Neuroimage. 2012;62(2):774-81.
29. Fischl B, Salat DH, Busa E, Albert M, Dieterich M, Haselgrove C, et al. Whole brain segmentation: automated labeling of neuroanatomical structures in the human brain. Neuron. 2002;33(3):341-55.
30. Desikan RS, Ségonne F, Fischl B, Quinn BT, Dickerson BC, Blacker D, et al. An automated labeling system for subdividing the human cerebral cortex on MRI scans into gyral based regions of interest. Neuroimage. 2006;31(3):968-80.
31. Jenkinson M, Smith S. A global optimisation method for robust affine registration of brain images. Medical Image Analysis. 2001;5(2):143-56.
32. Jenkinson M, Bannister P, Brady M, Smith S. Improved Optimization for the Robust and Accurate Linear Registration and Motion Correction of Brain Images. NeuroImage. 2002;17(2):825-41.
33. Avants BB, Epstein CL, Grossman M, Gee JC. Symmetric diffeomorphic image registration with cross-correlation: evaluating automated labeling of elderly and neurodegenerative brain. Medical image analysis. 2008;12(1):26-41.

34. Avants BB, Tustison NJ, Song G, Cook PA, Klein A, Gee JC. A reproducible evaluation of ANTs similarity metric performance in brain image registration. NeuroImage. 2011;54(3):2033-44.
35. Tournier JD, Smith R, Raffelt D, Tabbara R, Dhollander T, Pietsch M, et al. MRtrix3: A fast, flexible and open software framework for medical image processing and visualisation. NeuroImage. 2019;202:116137.
36. Andersson JLR, Sotiropoulos SN. An integrated approach to correction for off-resonance effects and subject movement in diffusion MR imaging. NeuroImage. 2016;125:1063-78.
37. Tustison NJ, Avants BB, Cook PA, Zheng Y, Egan A, Yushkevich PA, et al. N4ITK: improved N3 bias correction. IEEE transactions on medical imaging. 2010;29(6):1310-20.
38. Tournier JD, Calamante F, Connelly A, editors. Improved probabilistic streamlines tractography by 2nd order integration over fibre orientation distributions. Proceedings of the international society for magnetic resonance in medicine; 2010: John Wiley & Sons, Inc. New Jersey, USA.
39. Tournier JD, Calamante F, Connelly A. Robust determination of the fibre orientation distribution in diffusion MRI: Non-negativity constrained super-resolved spherical deconvolution. NeuroImage. 2007;35(4):1459-72.
40. Fortin J-P, Parker D, Tunç B, Watanabe T, Elliott MA, Ruparel K, et al. Harmonization of multi-site diffusion tensor imaging data. NeuroImage. 2017;161:149-70.
41. Fortin J-P, Cullen N, Sheline YI, Taylor WD, Aselcioglu I, Cook PA, et al. Harmonization of cortical thickness measurements across scanners and sites. Neuroimage. 2018;167:104-20.
42. Civier O, Smith RE, Yeh C-H, Connelly A, Calamante F. Is removal of weak connections necessary for graph-theoretical analysis of dense weighted structural connectomes from diffusion MRI? NeuroImage. 2019;194:68-81.
43. Zalesky A, Fornito A, Bullmore ET. Network-based statistic: identifying differences in brain networks. Neuroimage. 2010;53(4):1197-207.
44. MATLAB. MATLAB. version 9.6.0.1072779 (2019a) ed. Natick, Massachusetts2019.
45. Rubinov M, Sporns O. Complex network measures of brain connectivity: Uses and interpretations. NeuroImage. 2010;52(3):1059-69.
46. Latora V, Marchiori M. Efficient behavior of small-world networks. Physical review letters. 2001;87(19):198701.
47. Wang Y, Ghumare E, Vandenberghe R, Dupont P. Comparison of different generalizations of clustering coefficient and local efficiency for weighted undirected graphs. Neural computation. 2017;29(2):313-31.
48. Frossard J, Renaud O. Permutation tests for regression, ANOVA, and comparison of signals: the permuco package. Journal of Statistical Software. 2021 Oct 22;99:1-32. ANOVA/ANCOVA and Comparison of Signals. R package version 1.1.0. ed2019.
49. Kaye, Fudge, Paulus. New insights into symptoms and neurocircuit function of anorexia nervosa. Nat Rev Neurosci. 2009;10(8):573-84.
50. Park RJ, Godier LR, Cowdrey FA. Hungry for reward: How can neuroscience inform the development of treatment for Anorexia Nervosa? Behav Res Ther. 2014;62:47-59.
51. Walsh BT. The enigmatic persistence of anorexia nervosa. Am J Psychiatry. 2013;170(5):477-84.
52. Van Den Heuvel MP, Sporns O. Rich-club organization of the human connectome. Journal of Neuroscience. 2011;31(44):15775-86.

53. Vogel K, Timmers I, Kumar V, Nickl-Jockschat T, Bastiani M, Roebroek A, et al. White matter microstructural changes in adolescent anorexia nervosa including an exploratory longitudinal study. NeuroImage Clinical. 2016;11:614-21.
54. Frank GKW, Shott ME, Hagman JO, Yang TT. Localized brain volume and white matter integrity alterations in adolescent anorexia nervosa. Journal of the American Academy of Child and Adolescent Psychiatry. 2013;52(10):1066-75.e5.
55. Frank G, Shott M, Riederer J, Pryor T. Altered structural and effective connectivity in anorexia and bulimia nervosa in circuits that regulate energy and reward homeostasis. Translational psychiatry. 2016;6(11):e932-e.
56. Calamuneri A, Arrigo A, Mormina E, Milardi D, Cacciola A, Chillemi G, et al. White Matter Tissue Quantification at Low b-Values Within Constrained Spherical Deconvolution Framework. Frontiers in Neurology. 2018;9(716).